3rd ASME/IEEE International Conference on Mechatronic and Embedded Systems and Applications
MESA07
September 4-7, 2007, Las Vegas, Nevada, USA

DETC2007-34261

SPECIALISED IMAGE CAPTURE SYSTEMS FOR A DIET BREAST CANCER SCREENING SYSTEM

Christopher E. Hann
Department of Mechanical Engineering
University of Canterbury
Christchurch, New Zealand

J. Geoffrey Chase
Department of Mechanical Engineering
University of Canterbury
Christchurch, New Zealand

Crispen Berg
Department of Mechanical Engineering
University of Canterbury
Christchurch, New Zealand

Richard G. Brown
Department of Mechanical Engineering
University of Canterbury
Christchurch, New Zealand

Rodney B. Elliot
Department of Mechanical Engineering
University of Canterbury
Christchurch, New Zealand

XiaoQi Chen
Department of Mechanical Engineering
University of Canterbury

ABSTRACT

Digital Image-based Elasto-Tomography (DIET) is an emerging technology for non-invasive breast cancer screening. This technology actuates breast tissue and measures the surface motion using digital imaging technology. The internal distribution of stiffness is then reconstructed using Boundary Element or Finite Element Methods (FEM or BEM). However, obtaining accurate imaging at high frequency and high resolution in terms of numbers of pixels is challenging if enough accuracy is to be obtained in the motion sensing to deliver a useful result. The overall focus of such mechatronic and digitally centred systems is on providing a low-cost, radiation dose-free and portable screening system capable of screening numerous patients per day – in direct contrast to current low throughput, non-portable and high cost x-ray and MRI based approaches.

Thus, DIET technology relies on obtaining high resolution images of a breasts surface under high frequency actuation, typically in the range of 50-100Hz. Off-the-shelf digital cameras and imaging elements are unable to capture images directly at these speeds. A method is presented for obtaining the required high speed image capture at a resolution of 1280x1024 pixels and actuation frequency of 100Hz. The prototype apparatus presented uses two imaging sensors in combination with frame grabbers and a dSpace™ control system, to produce an automated image capture system. The system integrates a precision controlled strobe lighting system to selectively capture sinusoids at different points in the sinusoidal cycle of response.

The final working system produced images that enabled effective 3D motion tracking of the surface of a silicon phantom actuated at 100Hz. The surface of the phantom was strobed at pre-selected phases from 0 to 360 degrees, and an image was captured for each phase. The times at which image capture occurred were calculated for a phase lag increment of 10 degrees resulting in an image effectively every 0.00028s for the actuator cycle of 0.01s. The comparison of the actual trigger times and pre-selected ideal trigger times gave a mean absolute error of 1.4%, thus demonstrating the accuracy of the final system.

Final validation is performed using this system to track motion in a silicon gel phantom. The motion is tracked accurately using a novel Euclidean Invariant signature method. Both cameras delivered similar results with over 90% of points tracked to within 1-2%. This level of accuracy confirms the ability to effectively accurately reconstruct the stiffness as validated in other related studies.

INTRODUCTION

Breast cancer is a significant health problem in both developed and developing countries [1]. Mammography is currently the standard for breast cancer screening. However, it can cause significant discomfort to patients, requires radiation exposure and interpretation of images is subjective, potentially leading to misdiagnosis and false positives.

Digital Image-based Elasto-Tomography (DIET) is an emerging technology for non-invasive breast cancer screening. The DIET system uses digital imaging of an actuated breast surface to determine tissue surface motion from a specified input. It then reconstructs the 3D internal tissue stiffness distribution from that motion. Regions of high stiffness suggest cancer since cancerous tissue is between 3 and 10 times stiffer than healthy tissue in the breast [2-4]. This approach eliminates the need for X-Rays and excessive, potentially painful compression of the breast [5] as required in a mammogram. Hence, screening could start much younger and might enjoy greater compliance [6].

The internal property reconstruction methods have been developed using finite elements in both simulation and experimental cases [5,7], Boundary Elements in simulation [8] and Hybrid Optimisation in both simulation and experimental cases [9]. Results to date show the full potential to carry this task out in general geometries presuming the motion capture can be provided in detail, which is the focus of this work.

For optimal 3D tissue reconstruction, the breast is actuated at 50-100 Hz [10-11]. This frequency is well outside the frequencies of biological processes, such as breathing and heart rate. The amplitude of actuation is about 1-5 mm, which takes into account patient comfort, and limitations on actuator and motion measurements. At these high frequencies, image capture is therefore a challenging task, since clear, crisp images at high resolution are required for high density, accurate velocity and displacement vectors to be obtained. This requirement for the cameras puts the array of pixels required in the SVGA range (1264x1016), at minimum. Based on prior analysis of field of view size and desired spatial resolution, images of 4-16 Mpixels will be required [12].

This paper develops and implements a method for combining a stroboscope with "off the shelf" CMOS imaging sensors to enable high frequency high-resolution image capture for the DIET system. In particular, the KAC-9648 SVGA CMOS imaging sensors from Kodak are used and the image capture method developed in this research is shown to efficiently and automatically grab images from the breast with actuation frequencies of 50-100 Hz.

As a result, the need for very expensive high speed, high frame rate image capture, which often comes only at lesser resolution, is avoided. In particular, the approach presented allows low cost standard imaging sensors to be used. These sensors are growing in size (Mpixels) and speed on an annual base, so the approach presented allows this technology to be utilized as it appears rather than waiting for it to be used in high speed image capture systems.

This research uses CMOS imaging sensors due to their reduced size over their commercial CCD counterparts. This difference would allow the freedom of placing more cameras in a dense array to capture all actuated breast motion with very high resolution. This choice thus also enables greater imaging resolution to be obtained while maintaining simplicity or a lack of greater complexity, in the silicon technology used.

The overall approach is validated by tracking motion of artificially placed fiducial points on the surface of a silicon gel phantom. The motion tracking is performed based on a novel Euclidean Invariant signature [13], which compacts a large amount of information into a simple form. The signature is effectively invariant to the phantom's motion, thus the process of identifying points between images is transformed into a dramatically simpler problem of identifying the overlaps of two signatures. The end result is the ability to track large numbers of points very accurately and with minimal computation required. The high accuracy and resolution obtained in tracking ensures accurate tissue stiffness reconstruction.

IMAGE CAPTURE SYSTEM

Figure 1 shows a picture of the system. The setup for the new image capture system developed is divided into two main sections:

- Image Capture
- Actuator and Trigger Control

The overall layout for the image capture and related trigger and data lines is illustrated in Figure 2.

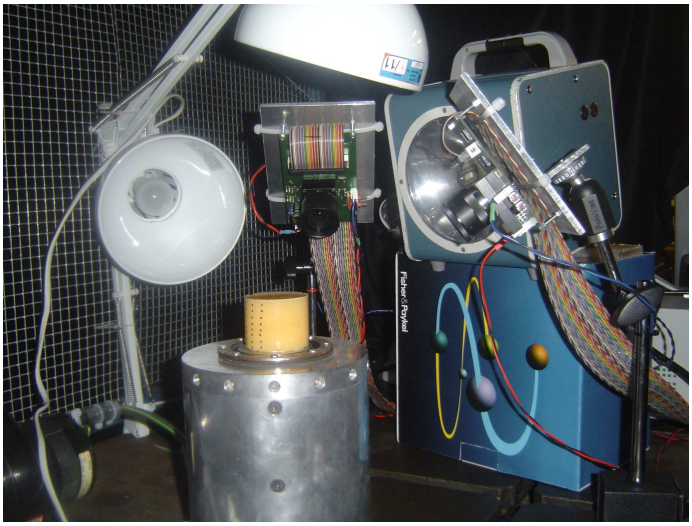

Figure 1: Image capture setup

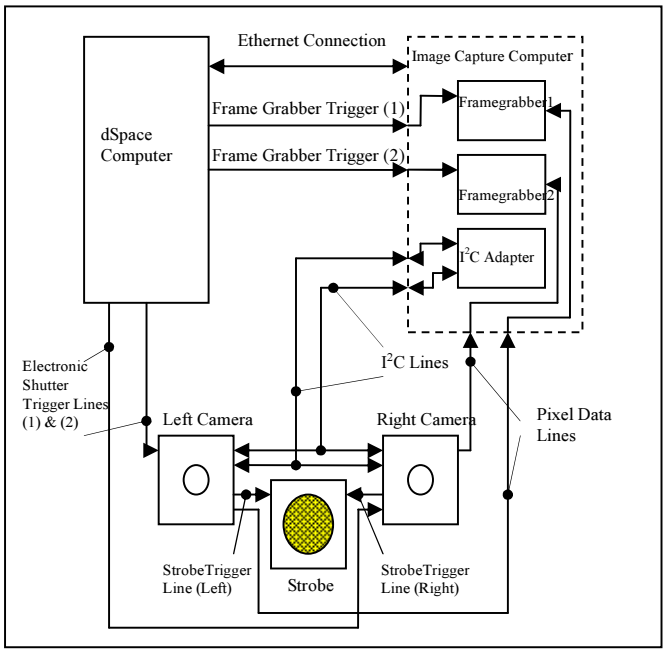

Figure 2: The layout for the digital image capture system

IMAGE CAPTURE

The image capture computer (ICC) handles all the capturing and storing of the digital images. The ICC contains two PCI frame grabbers and an I2C adapter. The PCI frame grabbers capture all the image data arriving from the imaging sensors along the pixel data lines, as shown in Figure 2. Two Kodak KAC-9648 colour image sensors are used in this apparatus. Each sensor produces image data output in the form of 10-bits per pixel at a resolution of 1280 x 1024. Communication between the image capture computer and the camera is carried out via the I^2C adapter. The adapter has two digital lines coming out of it, the first is the serial data line (SDL) and the second is the serial clock line (SCL).

Both cameras are connected in parallel to these two serial lines and each has a unique bus address. For example, when the I^2C adapter communicates with the left camera, it first transmits the bus address, of the left camera. This puts the camera in a state to listen for any information arriving down the two serial lines. This information could be a change in the active window size required by the user or same other input. The right camera then ignores this information since the I^2C adapter is only "addressing" the left camera.

There are two camera configurations required, involving a communication between the I^2C adapter and the cameras. The first camera configuration is the initialisation of the digital cameras, which enables them to be compatible with the frame grabbers. The result of this initialisation is a continuous stream of video data, which is displayed on the screen and enables the user to adjust colour gains, focus, camera position and aperture size as required.

The second configuration puts the cameras into a state where they are able to receive a digital pulse from dSpace™, which triggers the frame exposure and strobe activation. Specifically, there is an input pin and an output pin on the sensor that is automatically configured after instructions from the I_2C adaptor, as shown in Figure 3.

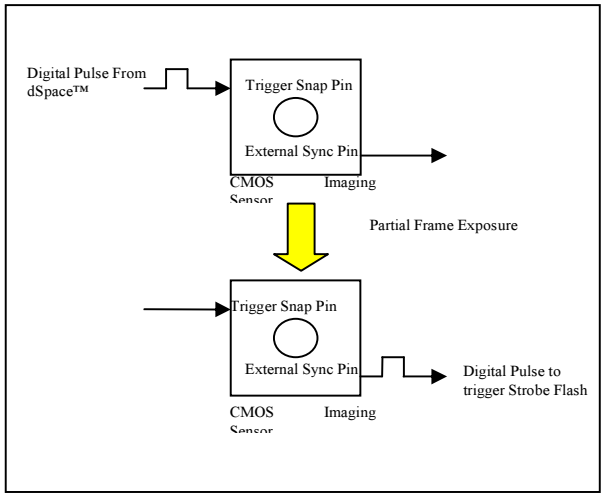

Figure 3: The process of strobe trigger by the camera

The first pin is called a triggered snap pin, which receives the pulse from dSpace™ and starts frame exposure. The second pin is called an external sync, which supplies a pulse to activate the strobe. The precise timing of the strobe trigger from the camera is preset and cannot be changed by the user.

After both camera configurations are performed, enabling compatibility with the frame grabbers and triggering of the frame exposure and strobe activation, the cameras are ready for image capture of the actuated test phantom.

ACTUATOR AND STROBE TRIGGER CONTROL

The set-up for the actuator and trigger control is shown below in Figure 4. The dSpace™ computer uses Simulink from Matlab™ to create a system for controlling the input and output signals. The system for processing the signals is built up from blocks, similar to a wiring diagram, where Simulink blocks are connected together to perform its portion of the image capture task on the dSpace™ module.

The portion of the image capture process for which the dSpace™ is responsible, is the generation and synchronising of signals sent to the actuator and necessary trigger signals. Once the diagram is ready it is automatically transferred to a C code format, uploaded to dSpace™, and then run by dSpace™ in real-time inside the dSpace™ module. The settings in the Simulink™ diagram can be adjusted in real-time using the dSpace™ software ControlDesk™. ControlDesk™ makes it

possible to automatically perform real time adjustments of the working embedded code in the dSpace™ module. For example, resetting the trigger signals to the frame grabbers and cameras, and real time adjustment of the actuator amplitude. ControlDesk also allows trigger settings to be modified via a user built project interface. The rounded boxes in Figure 4 represent the programs interactions with the hardware where ControlDesk™ and Matlab™ are constantly talking to one another and adjusting the settings in the dSpace™ module.

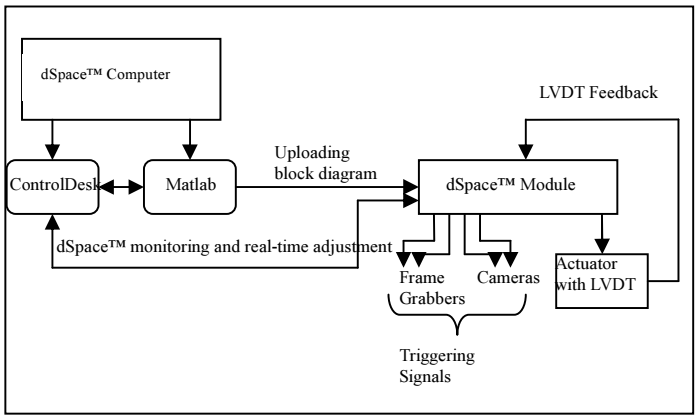

Figure 4: The process of strobe trigger by the camera

The programming language used to automate ControlDesk™ is known as Python. Python is a high level scripting, interpreted and interactive object-oriented programming language. The Python™ code is used to talk to the ICC and automate the sending of the trigger signals. The hierarchy for the operation of Simulink™, ControlDesk™ and Python™ can be seen in Figure 5.

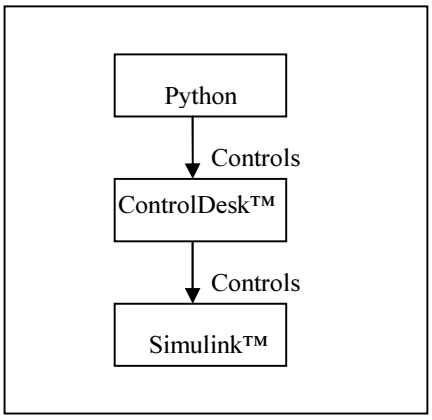

Figure 5: The hierarchy of control for the dSpace™ set-up

A 50-100 Hz sinusoidally (or periodically) actuated silicon phantom would require 50-100 fps in the imaging sensors. Since the frame rates of the CMOS imaging sensors for this project have a maximum rate of 18 fps at full resolution, it is therefore not possible to directly image the phantom. To overcome this problem the high-speed phantom is strobed at specific points in its motion, thus effectively rendering the object "stationary" at that point in its resulting sinusoidal periodic response.

In Figure 6 is an example of 12 different phase angles in the actuator's cycle where a user requires an image of the phantom. By introducing a phase shift between the actuators motion and the point of triggering the strobe, the object can be made "stationary" at each of these 12 user defined points in its response and thus an image taken.

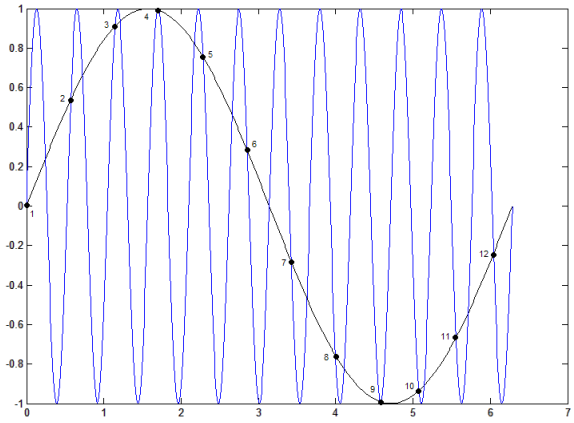

Figure 6: An example of a 12 Hz command signal that would drive the sinusoidal motion of an actuator.

In this example, the phase shifts are at increments of 30 degrees labelled 1 to 12 in Figure 6. A similar process could be used to capture images of an object at any predefined points in an actuator cycle for any actuator frequency.

For the DIET system, this provides the required ability to capture a sequence of high-resolution images of a 50-100 Hz actuated silicon breast phantom describing the displacement response throughout a 360-degree cycle. At each point the tissue surface motion is imaged and captured. From this data the magnitude and phase of the response relative to the input, can be readily obtained as it is assumed the small sinusoidal inputs result in a sinusoidal response at the (steady state) frequency.

The actuator used in this system has a linear transducer (LVDT), built into the core of the actuator, which sends data back to the dSpace™ module, see Figure 4.

PRELIMINARY IMAGE CAPTURE RESULTS

In the initial tests of the image capture set-up, the time period between when camera fired the strobe flash and the camera received the trigger pulse to snap a frame was

inconsistent and unpredictable. This inconsistency makes it very difficult to align the strobe trigger with the phase position in the actuators cycle. Specifically, consider the case of the actuator moving at a frequency of 100 Hz, which is the maximum frequency required of this image capture system. Thus, the actuator and silicon phantom move through a 360-degree cycle every 0.01 seconds. The problem is that while the time periods between the dSpace™ trigger pulse and the strobe trigger pulse are consistent at a time resolution of 0.1 seconds; it can fluctuate randomly over the finer resolution of 0.01 seconds. This behaviour is demonstrated in Figure 7 for the left camera over 7 images at a phase lag of 0-degrees and a 100Hz signal. In other words, the camera is not designed for precision strobing greater than 10 Hz image capture frequency.

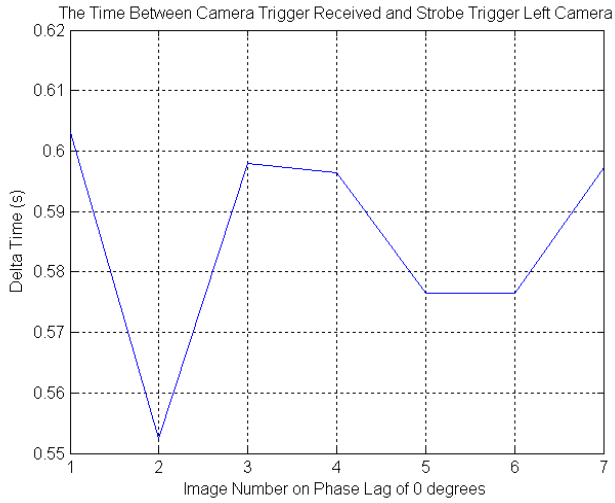

Figure 7: A graph of the dSpace trigger pulse/strobe trigger pulse time period

A second problem was also discovered involving external sync time variations between the two cameras. For example, triggering the strobe using the right camera resulted in partial images from the left camera on random phase lags. This problem was due to the left camera not being ready for the strobe to flash at the same time as the right camera, even though the dSpace trigger pulse was sent to the cameras at the same time.

CORRECTED IMAGE CAPTURE RESULTS

In this section the following problems are addressed and results presented:

- Inconsistencies in required strobe trigger between cameras
- An inconsistent time period, at the required time resolution, between the dSpace trigger pulse and the strobe trigger pulse

Both of these problems are addressed simultaneously with the introduction of solid state AND gate and a feed back pulse to the dSpace™ module, which triggers the strobe flash. As shown in Figure 8, the solid state AND gate is attached to the two external sync lines from each camera, and this addition aligns the two pulses into one coherent pulse that is fed into the dSpace™ module.

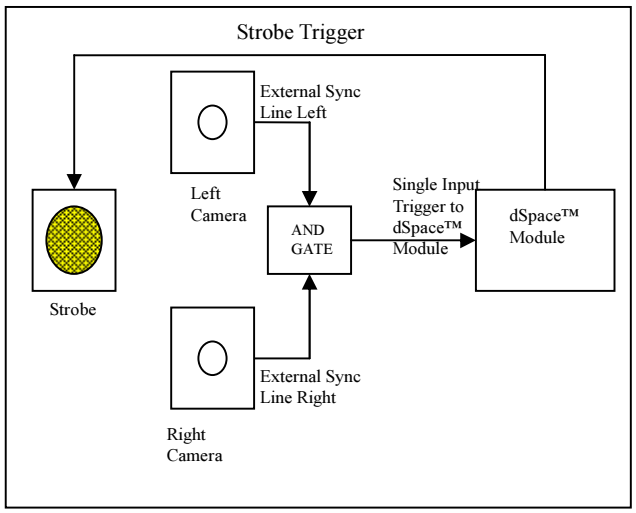

Figure 8: The new strobe trigger set-up

The single coherent external pulse sent to the dSpace™ module from the AND gate is then aligned with the rising edge of the now phase-lagged LVDT signal, which is then passed back out to trigger the strobe. The single external strobe trigger is aligned in much the same way as the camera snap trigger pulse using flip-flops Simulink™ blocks.

The strobe itself actually triggers on the falling edge of the trigger pulse and not the rising edge because of the way the strobe was designed by the manufacturer. Due to the falling edge trigger, a 'NOT' gate is used to invert the edge. The implementation of this 'NOT' gate achieves the result shown in Figure 5.6.

Each rising edge of the square wave LVDT lagged signal occurs at a specific point in the actuators motion. This rising edge is moved to other positions in the actuators motion, by adjusting the phase lag desired. It is this rising edge that the strobe must trigger on to capture the actuator at that specific position. The external sync from the cameras notifies the image capture system that the cameras are ready for the strobe flash, but the flash must occur on the rising edge of the lagged LVDT signal. Thus, the external sync must remain high until the next

rising edge in the lagged LVDT signal, which is at 0.01s intervals for 100Hz actuation.

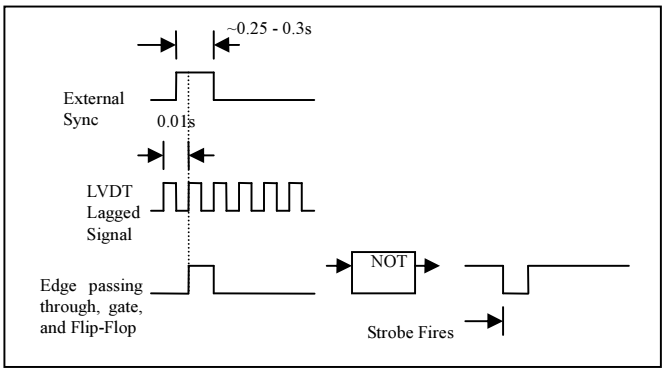

Figure 9: The timing of the modified strobe trigger

Since the external sync therefore may remain high for ~0.25-0.3s, there is plenty of time for the strobe to receive a rising edge and thus trigger a camera flash. The result of the solid state AND gate and feedback pulse to the dSpace™ module applied to the apparatus of Figure 2, allows the strobe to trigger at points close to the ideal trigger times as shown in Figure 10.

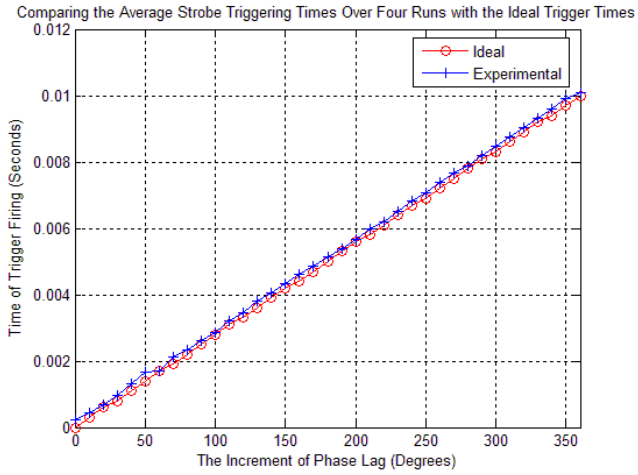

Figure 10: The comparison of the average strobe triggering times over the four image capture runs compared with the ideal triggering times.

It should also be noted that the actuator has imperfections or error in its motion. A snap shot of the actuators motion at t = 1.8207s compared with an ideal case given in Figure 11, shows a time period where the difference in the two waveforms is at a minimum corresponding to the best achievable actuator motion. The variation in frequency for Figure 12 is between ~98 to 100Hz or less than 2%.

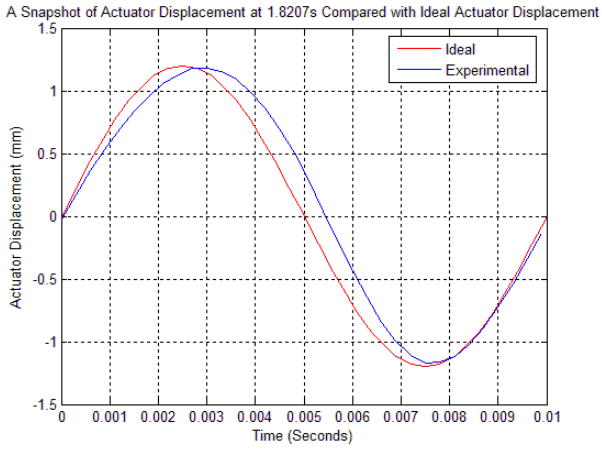

Figure 11: The actual position of the actuator compared to an Ideal position at a snapshot of the actuators motion taken at 1.8207 seconds.

An average of 20,000 actuator waveforms was taken, and the result is plotted in Figure 12 showing that a larger error dominates the motion. Since Figures 11 and 12 involve direct measurements of the actuator displacement, errors can be attributed to the dynamics of the actuator itself. In other words, there are physical limitations in the current actuator. Further experimental work and potential improvements need to be done in the future.

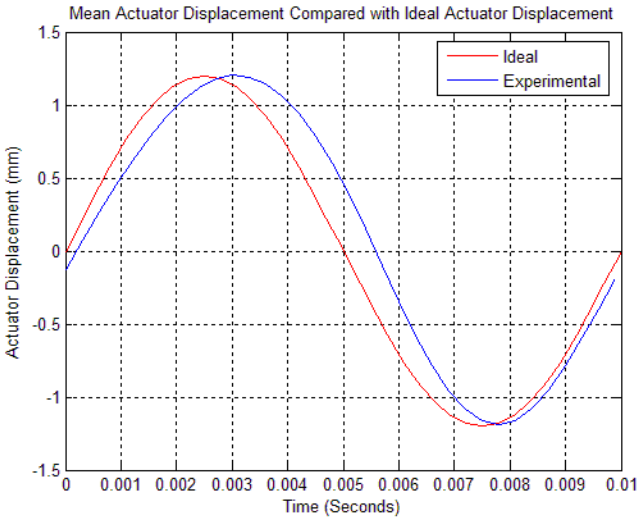

Figure 12: The mean actuator displacement compared with the ideal actuator displacement over 20,000 actuator cycles.

In practice, images of a silicon phantom's displacement response to one specific period of the actuator, as in Figure 11 for example, cannot be achieved. As discussed earlier, the way to build up one complete cycle of the actuated silicon phantom, is to strobe at pre-defined phase angles and capture an image at each strobed point in time. To further validate the method the phase lag increment is chosen to be 10 degrees so that strobing occurs every 0.00028s of the 0.01s cycle.

The actuator displacements at the time of the strobe firing are plotted in Figure 13. Note that the specific times that the images are taken can vary significantly between runs. However, relative to the 0.01s cycle the image capture times are very consistent, as shown in Figure 10. For example, the first 10 image capture times in Figure 13 are:

$$t = [5.541,14.5413,24.3915,34.1817,44.0121,$$
$$53.8224,63.6525,73.4427,83,2932,93.0834]$$

With respect to the 0.01s cycle the 10 image capture times are effectively:

$$t = [0.0002,0.0005,0.0007,0.001,0.0013,0.0016,$$
$$0.0017,0.002,0.0024,0.0026]$$

These values are very close to multiples of 0.00028, as required. The results in Figure 13 show similar behaviour to Figures 11 and 12, further demonstrating the accuracy of the strobe and camera trigger system.

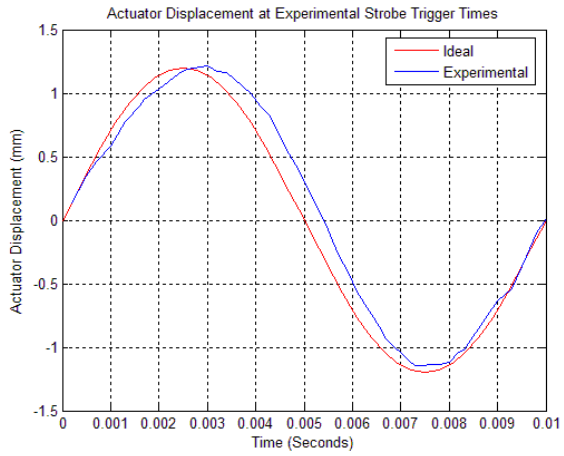

Figure 13: The compiled actuator displacements at the time of the strobe firing, compared with an ideal actuators displacement at that point.

SURFACE MOTION TRACKING

The system is first tested with a reasonably small number of points using a silicon phantom moulded in a cylindrical shape. The silicon phantom used in this experiment is a two-part mix solid silicon elastomer, and is shown in Figure 14.

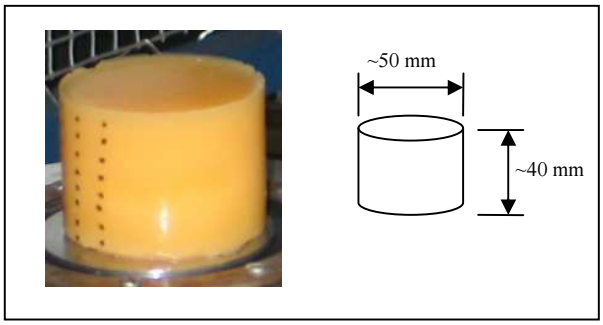

Figure 14: The silicon phantom used in the experiments and its dimensions

This silicon polymer was chosen because of similarities with the elastic properties of human tissue.

36 images are taken of the silicon phantom corresponding to 60 degrees intervals from 0-300 degrees, see Figure 15. The frequency of actuation is 100Hz with amplitude of 1.2mm. On the face common to both cameras there are 54 black dots, which are used to help track the surface motion of the phantom. The camera was calibrated beforehand by corresponding known points on a precisely machined calibration object with their image locations and solving for the projection matrix.

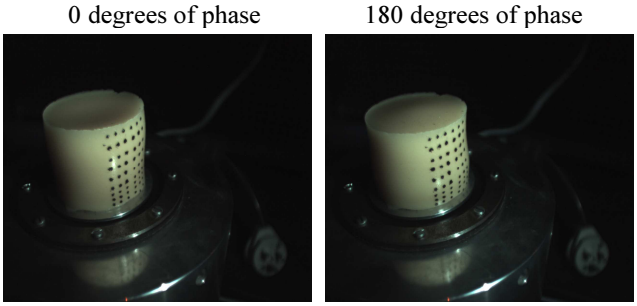

Figure 15: Two images of the silicon phantom from the left camera with 54 black dots on the surface moving at 1.2 mm of amplitude.

To validate the image capture system, the black dots in Figure 15 are used to track the displacement of the moving surface of the phantom. The motion tracking algorithm is based on [13]. Figure 16 shows the moving phantom and crosses overlaid by the image tracking algorithm. Figure 17 shows an example of the 3D tracked motion for one of the points in Figure 16. Note that a small number of the dots on the surface of the silicon phantom in Figure 16 could not be tracked because they move outside the field of view shared by both

cameras. An example of the reconstructed surface for one point in the actuators cycle is shown in Figure 18. The 3D mapped positions of the dots are then used to construct a virtual silicon phantom with the mapped dots displayed in red as shown in Figure 19.

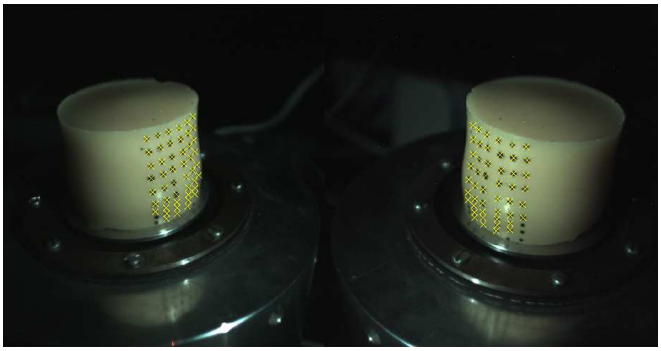

Figure 16: Tracking motion of the dots on the silicon phantoms surface, using images from the DIET image capture system. The identified dots are denoted by crosses.

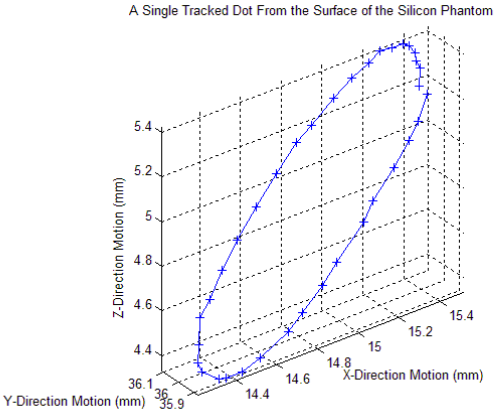

Figure 17: The motion of a single dot on the surface of the silicon phantom

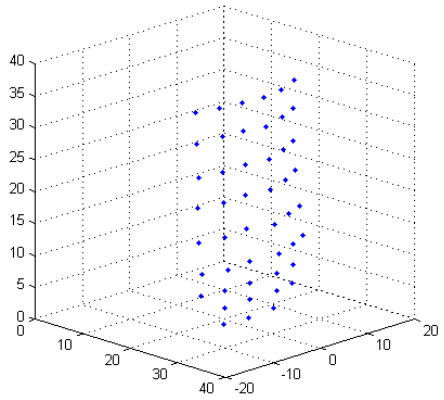

Figure 18: The 3D reconstruction of the tracked points from the phantoms surface

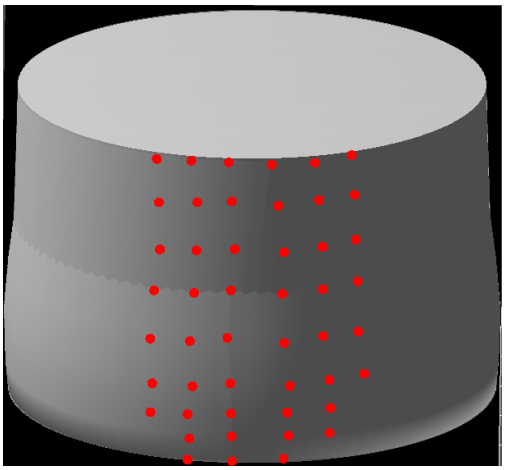

Figure 19: The virtual silicon phantom with the mapped points in red over the surface

The method is now tested on a new silicon phantom with significantly more points. Approximately 750 coloured points, 100 red, 300 blue and 350 green points were placed randomly on the phantom as shown in Figure 20. The phantom of actuated at 50 Hz, with 1mm peak to peak sinusoid at the actuator plate. A set of 20 images was captured to cover the entire sinusoid at 18 degree phase differences. The different coloured regions were found by thresholding the RGB image, and the positions of the points were found by the centroids of the coloured blobs.

An example of the extracted points is depicted in Figure 21. Note that with this simple approach not all the image points are recognised, however this is not a concern as only a certain density of points is needed to be matched, rather than every individual point.

(a) **(b)**

Figure 20: (a) Silicone gel phantom with coloured speckles. (b) detected red, green, and blue points.

The points in Figure 20 were then tracked using the Euclidean Invariant Signature approach of [13]. Figure 21 gives an example of the motion undergone by the matched points.

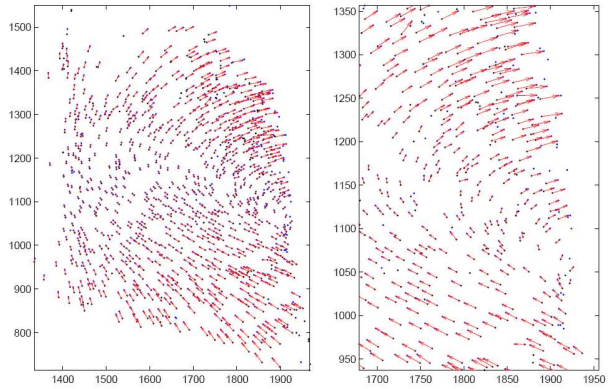

(a) **(b)**

Figure 21: Example of tracked points from gel phantom experiment, with matched pairs connected with an arrow. All the points are shown in (a) while (b) is a close-up

Over 90% of points in the images from both cameras were tracked successfully. Based on an estimate of the calibration accuracy of the cameras, the accuracy of tracking amounted to between 1-2% of the amplitude response for the silicon phantom.

CONCLUSIONS

A high-speed digital image capture system for Digital Image-based Elasto-Tomography (DIET) breast cancer screening has been presented. The final system satisfies the DIET system requirements of a completely automated relatively low cost method for capturing images of a silicon phantoms surface under sinusoid actuation at high frequencies of 50-100 Hz. The image capture system was successfully tested on silicon phantoms moving at 50 and 100 Hz and with amplitudes of 0.5 and 1.2 mm respectively. This provides accurate surface motion tracking at a high image resolution of 1280x1024. The image capture system also included functionality for the manipulation of colour gains and active windows making the system more adaptive to testing and laboratory conditions.

An important feature was the use of the dSpace™ control system module, which allowed the image capture process to take place outside of the Windows™ operating system message loops. This approach greatly increased the control over the timing of the events that go into capturing the high-speed images. It also more exactly matches any such commercial system, which would also use similar embedded operating system.

The construction of the digital cameras, in-house allowed a greater flexibility when it came to integrating them into the overall system. In addition, using Kodak's KAC-9648 CMOS imaging sensor, allows a reduction in complex circuitry in the camera design, simplifying making the future development and production of the digital cameras easier.

The comparison between the ideal and actual strobe triggering times, showed that the strobe was correctly triggered at the required predefined phase angles with a mean absolute error of ~1.4%. There were variations of the displacement of the actuator compared with the ideal actuator displacement at which the strobe triggers corresponding to a variation of 95-100 Hz within one image capture cycle. However, this displacement error was shown to be attributable to the dynamic properties of the actuator itself. For example, internal friction and the returning frequency of the LVDT signal varying slightly either side of the reference frequency for the introduction of the phase lag. A more exact next generation actuator will resolve these issues.

The time taken to complete an entire image capture run, of 37 images per camera took ~6 minutes upon review of the image capture log in the main application. This time can be reduced with the refining of the Ethernet protocols between the dSpace™ and image capture computer (ICC). The refining of the protocols could potentially reduce this image capture time by half (~3 minutes). Additionally, a custom designed system might reduce this test time by a further 2-10x.

REFERENCES

[1] I. S. Fentiman (2002). “Breast Cancer in Older Women”, Breast Cancer Online, Vol. 5

[2] A. Samani, J. Bishop, C. Luginbuhl, and D. B. Plewes (2003). "Measuring the elastic modulus of ex-vivo small tissue samples," Phys. Med. Biol., vol. 48, pp. 2183-2198, 2003.

[3] T. A. Krouskop, T. M. Wheeler, F. Kallel, B. S. Garra, and T. Hall (1998). "Elastic moduli of breast and prostate tissues under compression," Ultra-sonic Imaging, vol. 20, pp. 260-274.

[4] P. W. Wellman and R. D. Howe (2000). "Breast tissue stiffness in compression is correlated to histological diagnosis," Harvard BioRobotics Laboratory Technical Report.

[5] Peters, A, Milsant, A, Rouze, J, Ray, L, Chase, JG and Van Houten, EEW (2004). “Digital Image-based Elasto-Tomography: Proof of Concept Studies for Surface Based Mechanical Property Reconstruction,” Japanese Society of Mechanical Engineers (JSME) International Journal, Series C , Vol 47(4), pp. 1117-1123

[6] M. Robertson, "Commercialisation and IP Strategies for Digital Image-based Elasto-Tomography (DIET), MEM thesis 2005, University of Canterbury.

[7] Peters, A, Wortmann, S, Elliott, R, Staiger, M, Chase, JG, Van Houten, E (2005). “Digital Image-based Elasto-Tomography: First experiments in surface based mechanical property estimation of gelatine phantoms,” Japanese Society of Mechanical Engineers (JSME) International Journal, Series C , Vol 48(4), pp. 562-569

[8] Berger, H-U, Hann, CE, Chase, JG, Broughton, B and Van Houten, EEW (2007). “Boundary Element Methods in Elastography – A first explorative study,” Proc SPIE Medical Imaging Conf - Physiology, Function, and Structure from Medical Images, Feb 17-22, San Diego, USA, 12-pages.

[9] Peters, A, Chase, JG and Van Houten, EEW (2007). “Digital Image-based Elasto-Tomography: Combinatorial and Hybrid Optimization Algorithms for Shape-Based Elastic Property Reconstruction,” Physics in Medicine and Biology (PMB), IOP, accepted Dec 2006

[10] E.E.W. Van Houten, K.D. Paulsen, M.I. Miga, F.E. Kennedy and J.B. Weaver (1999). “An overlapping subzone technique for MR based elastic property reconstruction”, Magnetic Resonance in Medicine, 42(4), pp 779-786.

[11] E.E.W. Van Houten, J.B. Weaver, M.I. Miga, F.E. Kennedy and K.D. Paulsen (2000). “Elasticity reconstruction from experimental MR displacement data: Initial experience with an overlapping sub-zone finite element inversion process”, Medical Physics, 27(1), pp 101-107.

[12] A. Peters, A. Milsant, J. Rouze, L. Ray, J.G. Chase and E.E.W. Van Houten (2004). “Digital Image-based Elasto-Tomography: Proof of Concept Studies for Surface Based Mechanical Property Reconstruction”, Japanese Society of Mechanical Engineers (JSME) International Journal, Series C, Vol 47(4), pp 1117-1123.

[13] Brown, RG, Hann, CE, Chase, JG, and Ray, L (2007). “Discrete Colour-based Euclidean-Invariant Signatures for Feature Tracking in a DIET Breast Cancer Screening System,” Proc of the SPIE Medical Imaging Conference - Physiology, Function, and Structure from Medical Images, Feb 17-22, San Diego, USA, 12-pages